

Received August 2, 2020, accepted August 26, 2020, date of publication September 7, 2020, date of current version September 18, 2020.

Digital Object Identifier 10.1109/ACCESS.2020.3022213

Remote Thermal Water Leakage Sensor With a Laser Communication System

AMEEN AWWAD¹, MOHAMED YAHYA², LUTFI ALBASHA¹, (Senior Member, IEEE),
MD. MARUF MORTULA³, AND TARIG ALI², (Senior Member, IEEE)

¹Electrical Engineering Department, American University of Sharjah, Sharjah 26666, UAE

²GIS and Mapping Laboratory, American University of Sharjah, Sharjah 26666, UAE

³Civil Engineering Department, American University of Sharjah, Sharjah 26666, UAE

Corresponding author: Ameen Awwad (aawwad@aus.edu)


This work was supported by the Smart City Research Institute Grant at American University of Sharjah, UAE, under Grant EN-0282 and Grant OAP-CEN-066.

ABSTRACT The change in the temperature of an underground water pipeline and its surrounding environment caused by a leakage has been detected by a variety of devices. Among the most popular technologies are infrared cameras, distributed temperature sensing using fiber optic cables, and analog active temperature sensors. In this paper, a novel low-cost leakage detection system composed of two analog active temperature sensors is presented. The proposed system detects water leakages by comparing the readings of two analog active temperature sensors, one at the surface at a depth of 2 cm of a sand layer covering a buried water pipeline and the other is adjacent to the first sensor at the same depth in a thermally insulated portion by a polystyrene barrier. The results of the heat flow simulation developed with FEMM (Finite Element Method Magnetics) 4.2, which is free, open source, cross-platform capable of solving heat flow problems, showed that the addition of the insulation is expected to increase the difference between the readings of the sensors from 0.011 to 0.063 K (°C) when there is a leakage, and thus the addition of the insulation can be effective in making the effect of leaked water on the surface temperature more detectable. Experimental results indicated the capability of the proposed system in detecting water leakage which caused a temperature difference of 1.47 °C after 30 minutes of running a leaking water system. Furthermore, a laser communication system was built to allow for the transmission of an alarm signal from the sensing node above the underground pipeline to a master node which should have an internet connection to upload information to a cloud storage which can be accessed by different users.

INDEX TERMS Laser communication, leakage detection, Sustainable Development Goals (SDGs), temperature sensors, underground water pipeline.

I. LITERATURE REVIEW

Leakages in water distribution networks (WDNs) cause significant losses of treated water. The amount of lost water from WDNs in GCC (Gulf Cooperation Council) countries, the United Arab Emirates, Saudi Arabia, Kuwait, Qatar, Bahrain, and Oman, is about 30% of water supplied [1]. Specifically, in UAE, leaked water reaches 10% of water supplied [2], which is comparable to the loss percentage in Canada and USA of 13% and 16% respectively [3], [4] and the international average of best practice of 10 % [1]. Water leakages have two scenarios. First, when a water leakage appears on the surface of earth because of water capillarity

The associate editor coordinating the review of this manuscript and approving it for publication was Wei-Wen Hu .

or a burst due to high pressure. Obviously, in this scenario detection is easily done by inspection. However, this scenario is not likely to happen when the leakage is small, and the pipeline is buried at a depth of several meters. The highest point water can reach through capillary depends mainly on the aquifer system surrounding the pipeline which specifies the extent and patterns of groundwater flows. The main aquifer system in the UAE is divided into six regions as shown in Fig. 1. Sharjah, the understudy area, extends over two aquifers: the coastal Sabkhas and sand dune aquifer.

The most popular leakage detection technologies are ground penetrating radars (GPRs), acoustic detectors, and infrared (IR) cameras [5]. A GPR transmits radiofrequency (RF) waves to identify physical and chemical attributes of underground layers by measuring their different

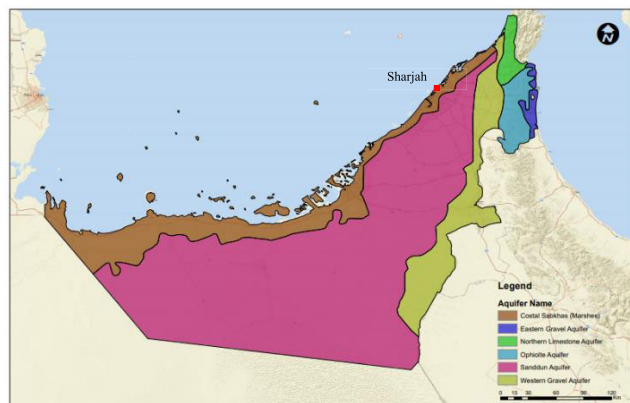


FIGURE 1. Main aquifer systems in U.A.E.

reflectivity and recording the travel time and power of the reflected signals. A GPR must go over the surface above a leakage to produce a 3D image of the volume of water leaked, where, as it passes above it, many 2D slices of the subsurface are captured, and then can be combined to form a 3D image [5]. Secondly, acoustic detectors sense leakage's mechanical noise produced by streaming water using various sensors, such as a pressure sensors, accelerometers, or hydrophones, which are deployed on the pipeline or inside it [6]. Moreover, ground microphones (geophones) can be used to detect underground leaks from the surface above the pipeline or from monitoring valves or fire hydrants [7]. The type of sensor is selected based on the material, diameter and configuration of the inspected pipeline [7]. An acoustic detector incorporates complex filtering and analysis system to discriminate the noise of a leakage from other high-intensity electromagnetic and ultrasonic sources in the environment, where the noise of leakages usually possesses some distinct characteristics, such as consistent amplitude over time, that facilitate signal processing [8]. Additionally, frequency analysis can help in distinguishing the acoustic emission of a leakage from other noises [6]. Finally, the change in the temperature of an underground water pipeline and its surrounding environment caused by leakages from underground WDNs the physical quantity measured by a variety of leakage detection technologies [9] – [14]. These technologies differ in accuracy, sensitivity to environmental conditions, and means of deployment with respect to the material inside the pipeline and the environment surrounding it. One of the most recent technologies is IR cameras, which rely on the change in temperature of the surface above the water leaked as it rises by capillarity through the subsurface [15]. IR cameras comes with low and high resolutions. IR cameras with low resolution, such as 80×60 pixels, proved effective in detecting leakage from underground water pipelines [9]. However, devices with higher resolution, specifically 320×240 pixels, proved to be more accurate in pinpointing the location of leakages [9]. High resolution IR cameras, such as ThermoCAM P60 with a resolution of 320×240 pixels, used in

leakage detection in [11], can detect temperature differences as small as $0.08 \text{ }^\circ\text{C}$ with an accuracy of $\pm 2 \text{ }^\circ\text{C}$ [16]. Additionally, IR cameras have shown the capability of detecting gas leaks [17]. A more mature technology is the distributed temperature sensing (DTS) system, which uses fiber optic cables to detect changes in the temperature caused by leakages which causes variations in the reflection of light in fiber optic cables and its wavelengths [12]. In this technology, optic cables are either mounted directly on the pipe [13], or a few feet away from it [12]. Therefore, unlike IR cameras, it requires excavation when installed for pipelines buried at a depth of several meters below earth. Typical DTS systems have an accuracy within $\pm 1^\circ\text{C}$ and a resolution of 0.01°C [18]. Similar to IR cameras, this technology can detect gas leaks [13], [19]. In a time-domain reflectometry (TDR)-based water leakage detection system, a metallic cable, instead of a fiber optic one, is extended along the surface above a “metallic” underground pipeline [20]. However, unlike DTS systems, this system measures the reflection coefficient between the metallic cable and the inspected underground pipeline which can be affected by the high permittivity of leaked water and has no relation to the working principle of thermal leakage detectors. Finally, analog active temperature (AAT) sensors, which requires external power source and outputs continuous signal, have been used in multiple leakage detection systems [14]. Multiple sensors can be connected either directly to the internet, specifically a cloud network [21], [22] where information would be accessible to multiple users, or indirectly through a master node [12], [14]. In [14], the system had a temperature sensor, LM35, attached on a medium-density polyethylene (MDPE) pipe while another temperature sensor was located approximately 30 cm away from the first one to measure the surrounding soil's temperature every 17 minutes. These sensors were connected to a sensor node fixed on the pipe, which transmits information via RF communication channels to a master node connected to the internet. In that study, results showed a significant drop in the temperature reading of the sensor attached on the pipe affected by water leaked, while the reading of the sensor placed away from the pipe varied slightly. An LM 35 sensor have an accuracy within $\pm 0.5 \text{ }^\circ\text{C}$ and resolution of $0.01 \text{ }^\circ\text{C}$ [23].

II. INTRODUCTION

Experts from Sharjah Electricity and Water Authority (SEWA) expressed dissatisfaction with the usage of the traditional acoustic leakage detection methods because of high acoustic noise in the field. Therefore, an alternative thermal detection system is presented. The low price of AAT sensors, relative to previously mentioned thermal sensors, makes it the most suitable for a large-scale smart leakage detection system. In this study, a sensing system with LM35 sensors for a large-scale smart leakage detection system for the SEWA's WDN in the sand dune aquifer of UAE.

The system in [14] connected several sensor nodes along the pipeline using PIC16LF1827 microcontroller and

433 MHz transceivers with a master node that should have internet connection to upload information to a cloud storage which can be accessed by different users. Though 433MHz RF link can be used by Arduino Uno, a laser communication system, that consists of a low power laser diode and photoresistor, is used between the sensing and master nodes because of their relative low cost. Because of this aspect, low cost, laser diodes have been part of IoT (Internet of Things) systems [24], and optical sensors in general [25], [26]. The laser communication system was developed to allow for the transmission of an alarm signal from the sensing node above the underground pipeline to a master node which should have an internet connection. The novelty of the proposed leakage detection system is not in its laser communication system, but mainly in its ability of detecting leakage at the surface above a WDN without the need of excavation to install AAT sensors on the underground pipeline itself nor close to it like the sensors in [14]. Moreover, the existence of the sensor node above ground in the proposed system, make replacing its battery easier. When the access to the sensor node is difficult, applying wireless power transfer techniques to recharge the battery can be alternative to replacing it, where inductive coupling has been widely used in such case [27]–[29], and especially in powering underground sensors where the magnetic field is not subject to absorption and scattering by soil, rocks and water, unlike the electromagnetic field [30], [31]. However, the efficiency of inductive coupling decreases exponentially with depth as the magnetic field intensity decreases [32]. Therefore, for the understudy WDN where the pipeline is buried at a depth of several meters, it is preferable for the sensor node to be on the surface.

There are various techniques for emulating a leaking water pipeline. These techniques include soft (computational) and mathematical models that can be a stand-alone prototype [33]–[35], or serve as a complementary part of a physical prototype [36]. Hard (physical) prototypes that replicate buried pipelines differs in their structure in accordance with the leakage detection system to be tested. Some of these prototypes are built to test the effectiveness of ground penetrating radars (GPRs) in detecting underground leakages. These prototypes consist of wooden tanks filled with soil where PVC pipes are buried [37], [5]. The wooden box can be constructed without the usage of metals such as screws and nails to avoid interference with radar signal during GPR scanning [37]. On the other hand, in the testing of acoustic methods, which depends on detecting the acoustic waves produced by leaking water, experimental setup was noticed to be installed in an outdoor field [38], [39]. Probably, an outdoor field is more suitable for applying acoustic methods than laboratory environment in the existence of several sources of acoustic noise. Water can be pumped from water grid when being in a laboratory, whereas, in an outdoor field, it is pumped from a tank placed near the testing location [39]. Finally, testing of thermal leakage detection systems through the thermal effect of leaked water on the surface of surrounding soil, was noticed to be conducted in both outdoor and laboratory

environments where the experimental setup consisted of a box made of wood or other material and filled with soil under which a plastic pipe is buried [9], [10], [14]. In this paper, the testing of the proposed AAT sensing system was carried in both soft and hard prototypes the characteristics of which is detailed in the next section. This study is part of our research for designing a sustainable water distribution network supporting the 11th Goal of the UN's Global Goals, also known as the Sustainable Development Goals (SDGs), which aims to “make cities and human settlements inclusive, safe, resilient and sustainable.”

III. RESEARCH METHODOLOGY

The design of the proposed leakage detection system is the outcome of intensive literature review, experts' opinions, and testing and analysis based on soft and hard prototypes.

For the soft prototype, the freeware FEMM (Finite Element Method Magnetics) 4.2, which is free, open source, cross-platform capable of solving heat flow problems, was used to develop a 2D cross-sectional model of the available hard prototype to test the performance of the proposed system. The schematic used had a depth of 0.01 cm representing a cross-section of the hard prototype starting from the surface of the pipeline up to the surface of the covering sand layer, as shown in Fig. 2.

The experimental work was carried using a hard prototype pipeline network to assess the proposed system reliability. The experimental setup was designed to replicate the existing conditions of the underground leaking pipes in sand dune part of Sharjah, where a centrifugal pump of 0.75 hp was connected to a 3.8-cm Polypropylene (PPR) pipe buried in a 101.6 × 34.3-cm wooden box at a depth of 40.6-cm, and an adjacent closed plastic water reservoir. The pressure in the pipe was less than 250 kN/m². Fig. 3. illustrates the number of times (cycles) the compactor was passed over the sand to reach the desired compaction level. The degree of compaction of dune sand was calculated to be 90%. Since main water pipelines in Sharjah is buried at 2 m below the ground surface or deeper, our system's scale factor is 4.92 (1cm:0.05m). The leakage detection system was connected to a computer to record temperature readings, although the computer is not part of the actual proposed system. These readings allowed the calibration of detection alarm, which be explained in the next section. A similar setup was used earlier to detect leakages using a ground-penetrating radar (GPR) and spectrometer [40], [41].

IV. PROPOSED SYSTEM ARCHITECTURE

A. STRUCTURE OF SENSOR AND MASTER NODE

Since a leakage causes a temperature anomaly on the surface above the damaged pipeline, thermally insulating a portion of the sand in the affected area by a polystyrene foam barrier, with the dimensions mentioned in the caption of Fig. 4 (a), and comparing the temperature at the surface of the insulated portion and the area affected by the leakage can make the detection of the leakage possible even if the sensing node does

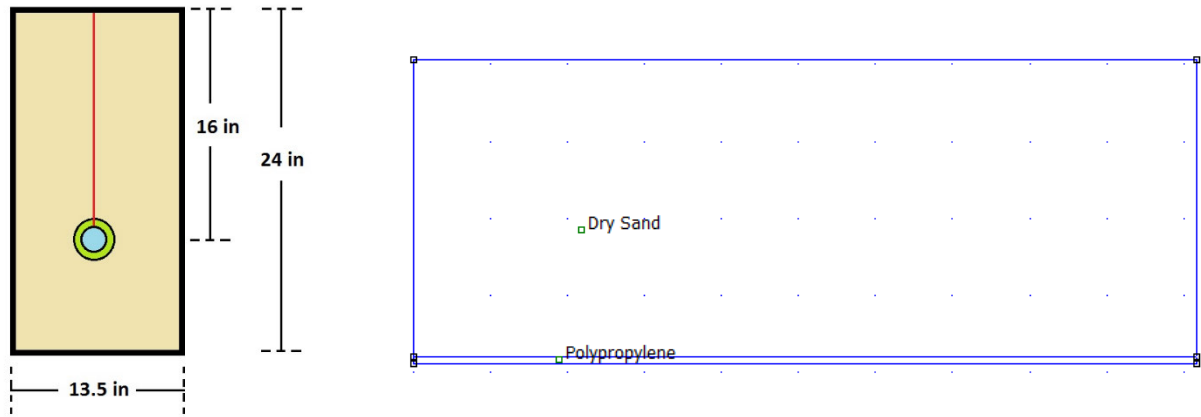


FIGURE 2. To the left, an illustration of a cross-section of the hard prototype perpendicular to the pipe central axis, where the red line represents the position of the cross-section parallel to the pipe used to draw the schematic to the right with FEMM.

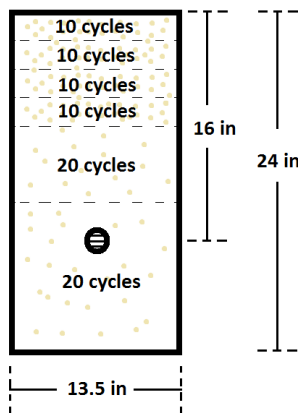


FIGURE 3. Compaction pattern.

not have previously a database of the natural temperatures of the sand at the surface. In the proposed system, the temperatures at the open area and insulated portion are measured by two LM35 temperature sensors. Fig. 4 shows the structure of the sensor node. An Arduino Uno board was programmed to set off an alarm signal when the temperature difference measured by the two LM35 sensors, 5.4 cm away from each other and buried at a depth of 2 cm, reaches or exceeds a certain value, measured during the experimental work to be 1.47 °C. The program placed on the microcontroller can be found in the Appendix. The laser communication system between the sensor node and master node consists of a low power metal enclosed laser diode, with a maximum transmission power of 5 mW at the sensor node side, and a photoresistor at the master node. Furthermore, since the photoresistors is sensitive to external light sources other than the laser beam, it was placed in a black paper hollow cylinder to allow for the passing of the directed laser beam only. The diameter of a laser beam increases from initial (ω_0), at its focus (double the distance from the center at which the beam's intensity

is $1/e^2$ (0.135) times its maximum value), to $(\sqrt{2}\omega_0)$ over a certain distance called the Rayleigh range (b), and then starts diverging by an almost constant angle. The Rayleigh range is given as follows [42]:

$$b = \frac{\pi * \omega_0^2}{\lambda} \tag{1}$$

where λ is the beam's wavelength. Since the Rayleigh range is inversely proportional to the wavelength (λ), it is minimum when the wavelength is maximum. The laser diode used can produce a wavelength range between 640 and 660 nm with a beam diameter at the focus of 5 mm. Thus, the laser beam diameter is expected to be approximately constant along the diode's range of operation, a few hundreds of meters between the sensor and master node, where the minimum Rayleigh range is around 24 km. In the prototype, the distance between the focus and the photoresistor was 1.8 m. In light, when a laser diode directed on the warped photoresistor used is off, its resistance is 2.3 M Ω . Fig. 5 (a) shows a schematic of the receiving device to which a master node should be connected, while Fig. 5 (b) shows the schematic used for simulating it as a transient circuit built with the free-software integrated circuit simulator Quite Universal Circuit Simulator (Qucs), which initially was created to be primarily an RF circuit analysis package which offered features not found in SPICE [43]. When 4 V is applied to the photoresistor connected in series with a 1k Ω resistor, negligible voltage drops across the 1k Ω when the laser diode in the transmitter is off, and the diode in the receiver remains reverse biased. However, when the laser diode is on, the photoresistor's resistance decreases to around 1 k Ω , and the voltage across it increases to half of the voltage applied forward biasing the diode to charge the capacitor. The usage of the capacitor allows a microcontroller in the master node to detect the laser pulse when the sensing node and master node are not synchronized keeping the analog input port on for a period longer than the short length of the laser pulse which is 1 ms in our case.

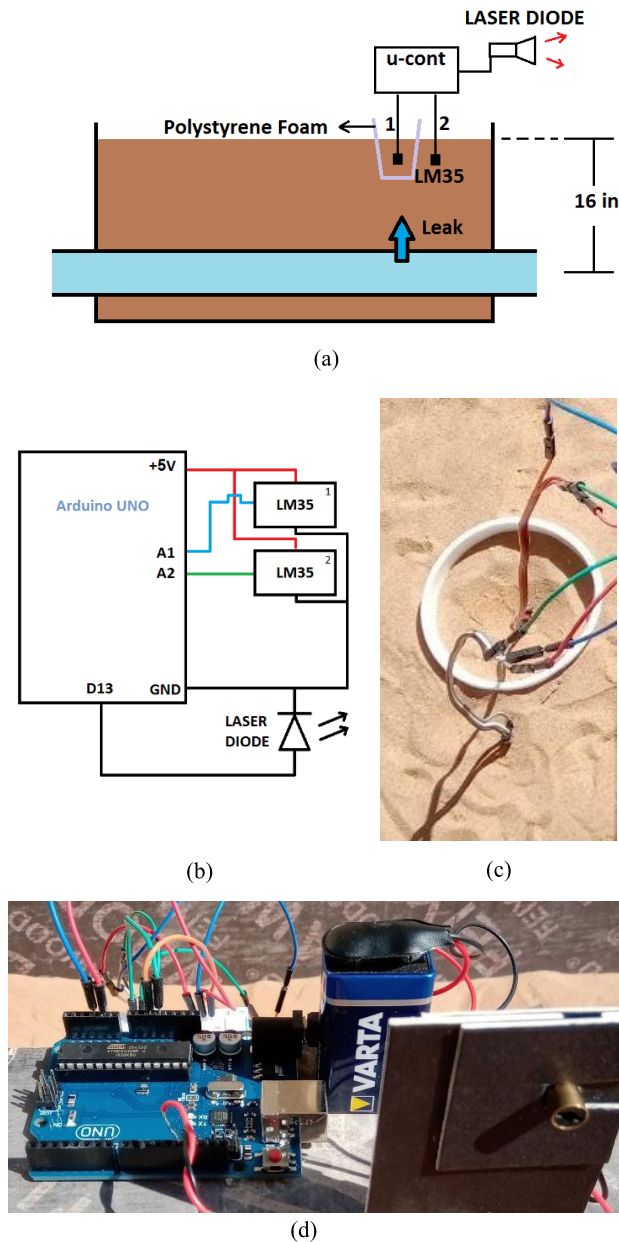
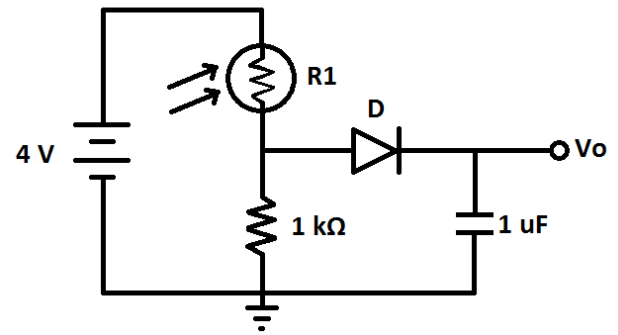
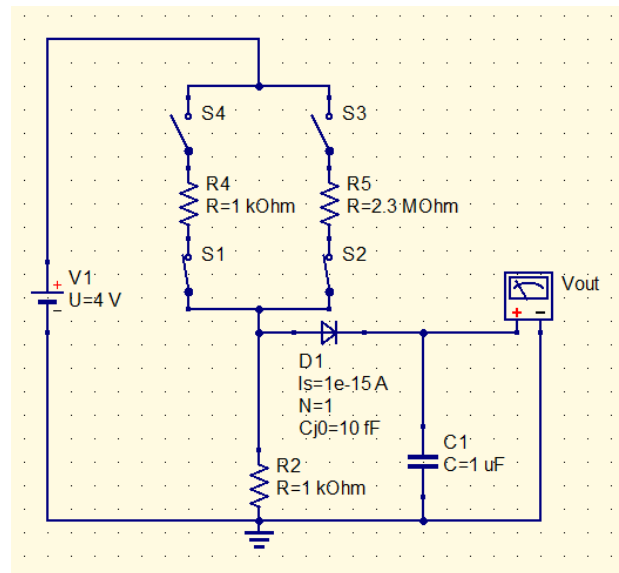


FIGURE 4. (a) Schematic of the sensing node (The insulator which has a shape of a cup with a thickness of 3 mm, height of 83.7 mm, and upper and lower diameters of 72.9 mm and 44.9 mm, respectively) (b) circuit of the sensor node (c) buried LM35 sensors (d) picture of the sensor node built (the LM35 sensors is buried in the soil).

The charging of the capacitor stops when the voltage across it reaches a value equal to the voltage across the 1 kΩ and diode, around 2.7 V, or when the laser pulse stops illuminating the photoresistor. The duration of the laser pulse is chosen in accordance with the capacitance used so that enough voltage develops across the capacitor during charging time where it will start discharging after the laser beam stops through the reverse biased diode and its internal resistance. Thus, we need to ensure that it will maintain the voltage for a long enough duration for the master node to recognize it. Although that



(a)



(b)

FIGURE 5. (a) The receiving circuit built that should be connected to the master node from the node Vo (b) the simulation of the circuit in (a).

discharging imposes a challenge, it allows receiving several laser pulses coming from different sensing nodes where each node should be dictated a certain period to transmits an alarm signal after the capacitor discharges the charge gained by receiving a previous laser beam.

The laser communication system’s simulation result that the capacitor should acquire a voltage of 1.12 volts. In the experimental testing of the circuit, a voltage around 1 volt was read across the capacitor after illuminating the photoresistor with a 1 ms laser pulse and then started to discharge to zero in around 15 seconds through the reverse biased diode and its internal resistance as mentioned earlier.

B. POWER CONSUMPTION OF SENSOR NODE

In idle mode, the sensor node drew 40 mA from an industry standard 9 V battery. Thus, the sensor’s idle mode’s power consumption is 360 mW. An analog input port of an Arduino Uno board has an operating voltage of 5 V, draws

40 mA [45], and takes about 100 microseconds to be read by the microcontroller [46]. Hence, the temperature reading process add a power consumption of 200 mW, and consequently, the total power consumption when the detector is active is 560 mW, where sensors will be read consequently. The detector would need to take a reading every 30 minutes as discussed in the next section. The laser diode was measured to draw 20 mA at 4.17 V, thus 83.4 mW, from the digital output port (D13) in on steady state condition. Then, a 1-ms laser pulse would consume approximately 23.2 nWh. Therefore, each idle mode cycle, which takes 30 minutes, consumes 0.18 Wh, whereas reading the two sensors, which takes 200 microseconds in active mode, consumes 31.1 nWh. Therefore, since an industry standard 9 V battery has an energy storage of 5.49 Wh [47], the sensor node would last about 15.25 hours. The power consumption of the sensor node is high relative to the power consumption of the sensor node in [12], equal to 2.2 μ W. This is because an Arduino Uno board is not made for power-efficient applications. However, it was used for its convenient connections as the focus in this study is the sensing mechanism.

V. PIPELINE SOFTWARE MODEL DEVELOPMENT

In the software model, each material had two parameters: thermal conductivity and volumetric heat capacity. Polypropylene thermal conductivity is 0.14 W/(m*K) [48]. Since the volumetric heat capacity of polypropylene varies with density, it was estimated to be 0.6385 MJ/m³/K by measuring the density of the pipe used in the experiment (336.1 kg/m³) and multiplying it with the specific heat of polypropylene (1.9 kJ/(kg*K)) [48]. For the expanded polystyrene foam barrier, the minimum thermal conductivity is 0.035 W/(m*K) [49]. Similar to polypropylene, the volumetric heat capacity was estimated to be 0.0246 MJ/m³/K by measuring the density of the cup used in the experiment (16.4 kg/m³) and multiplying it with the specific heat of polystyrene (1.4 kJ/(kg*K)) [48]. The leaked water from the damage of the pipeline was simulated as a circular area, as shown in Fig. 6 (a), in accordance with the images of the evolution of water leakage in dry soil captured and processed with a ground penetrating radar (GPR) [50]. where though the movement of leaked water through soil doesn't follow an uniform shape, a spherical diffusion from the leakage point is noticed. The head of saturated sand column in the model, due to the mixing of leaked water and surrounding sand, was deduced from the capillary rise of water in fine sand, which is 21 cm [50]. The initial water temperature over that medium is set equal to the temperature inside the pipe, measured to be 311.15 K (38 °C) in the experimental apparatus. Because sand temperature varies vertically with depth, it is virtually divided into ten layers, each is 2.1 cm thick, as shown in Fig. 6 (a). The lines dividing the inner area of the half circle have no boundary conditions and is to be removed before starting the simulation because it is drawn for demonstration only. The boundary condition at the bottom where given the temperature of water inside the pipe, equal

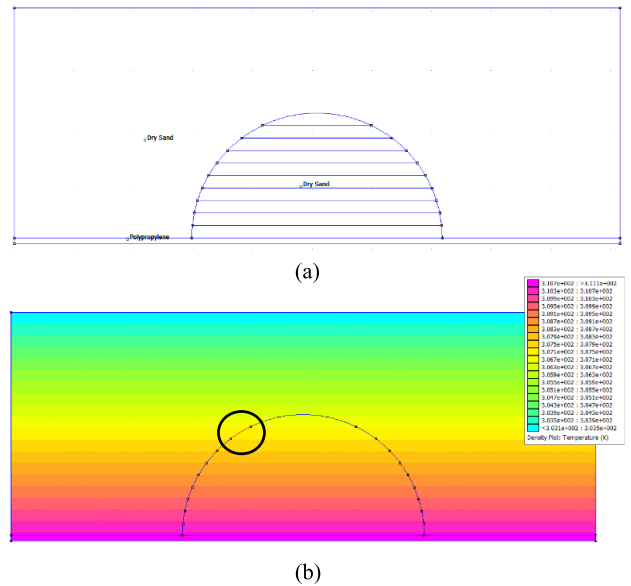


FIGURE 6. (a) Primary schematic used for simulating a water leakage in an underground pipeline (b) the result of the first simulation; one of the arcs along which an average temperature was calculated, using the integration tool, is indicated with red and circled.

to 311.15 K (38 °C) as mentioned previously, while at the upper most line of the model, the temperature was set to the expected ambient temperature during the experimental work (303.15 K (30 °C)). No boundary conditions were applied to the outer vertical sides because in the experiment these sides were loosely thermally insulated with wooden walls. The initial temperature (t_{wi}) at the sides of each layer (i) was estimated by integrating the average temperature along the arc length of each segment, as shown in Fig. 6 (b). The upper most segment had only one arc while the others had two on their sides. Assuming the heat lost from water (Q_w) in the saturated sand medium is equal to that acquired by sand molecules (Q_s) in the same medium, the arcs of each segment was given the final temperature calculated with equation (9) derived as follows:

$$Q_w = -Q_s \tag{2}$$

$$m_w c_{pw} \Delta t_w = -m_s c_{ps} \Delta t_s \tag{3}$$

$$m_w c_{pw} (t_f - t_{wi}) = -m_s c_{ps} (t_f - t_{avg,i}) \tag{4}$$

where m_w and m_s are the masses of water and sand respectively in the concerned segment, c_{pw} and c_{ps} are the specific heat capacities of water and dry sand, Δt_w and Δt_s are the changes in the temperature of water and sand, respectively, and t_f is the final temperature of both of water and sand when heat transfer stops and $t_{avg,i}$ is the average temperature along the arc length of the corresponding sand layer (i).

$$t_f = \frac{m_w c_{pw} t_{wi} + m_s c_{ps} t_{avg,i}}{m_w c_{pw} + m_s c_{ps}} \tag{5}$$

$$t_f = \frac{V_w D_w c_{pw} t_{wi} + V_s D_s c_{ps} t_{avg,i}}{V_w D_w c_{pw} + V_s D_s c_{ps}} \tag{6}$$

TABLE 1. Initial and final temperatures of each layers numbered from the top layer in ascending order.

Layer (i)	t_{si} (K)	t_{si} (°C)	t_{fi} (K)	t_{fi} (°C)
1	306.811	33.661	309.1389	35.9889
2	307.285	34.135	309.3586	36.2086
3	307.707	34.557	309.5542	36.4042
4	308.125	34.975	309.7479	36.5979
5	308.543	35.393	309.9417	36.7917
6	308.961	35.811	310.1354	36.9854
7	309.378	36.228	310.3287	37.1787
8	309.795	36.645	310.522	37.372
9	310.223	37.073	310.7203	37.5703
10	310.63	37.48	310.909	37.759

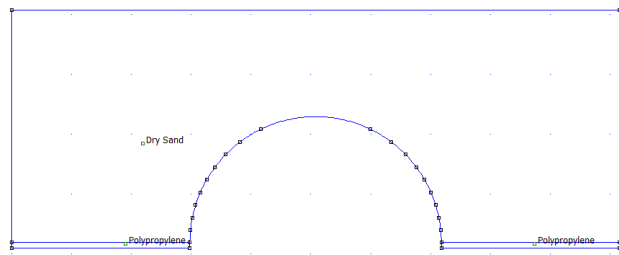


FIGURE 7. Primary schematic used for producing the heat flow diagram after estimating the leakage effect.

where V_w and V_s are the volumes of water and sand, and D_w and D_s are the densities of water and dry sand, respectively. By multiplying specific heat capacity of each material with its density, we get the volumetric heat capacity:

$$t_f = \frac{V_w c_{pVw} t_{wi} + V_s c_{pVs} t_{avg.i}}{V_w c_{pVw} + V_s c_{pVs}} \quad (7)$$

where c_{pVw} is volumetric heat capacity of water, equal to $4.18 \text{ MJ/m}^3/\text{K}$, and c_{pVs} is volumetric heat capacity of sand, around $1.3 \text{ MJ/m}^3/\text{K}$ for sand with no water content according to the volumetric heat capacity graph in [51]. Assuming the sand will reach retention in the area affected by leaked water, the water content level is likely to reach 0.36 according to the retention curves in [52], [53]:

$$t_f = \frac{0.36 V_s c_{pVs} t_{wi} + V_s c_{pVs} t_{avg.i}}{0.36 V_s c_{pVs} + V_s c_{pVs}} \quad (8)$$

$$t_f = \frac{0.36 c_{pVw} t_{wi} + c_{pVs} t_{avg.i}}{0.36 c_{pVw} + c_{pVs}} \quad (9)$$

Table 1 lists the initial and final temperatures of each layer.

Fig. 7 shows the primary model used for producing the heat flow diagrams of the leakage, where the sand and pipe wall below the boundary of the saturated sand are removed because the sand layer above the leakage area will be affected by the boundary temperature of the saturated sand where the sides of each segment in it is given the corresponding final temperature in Table 1. A polystyrene cup was added in both leak and no leak conditions. This addition was made to study

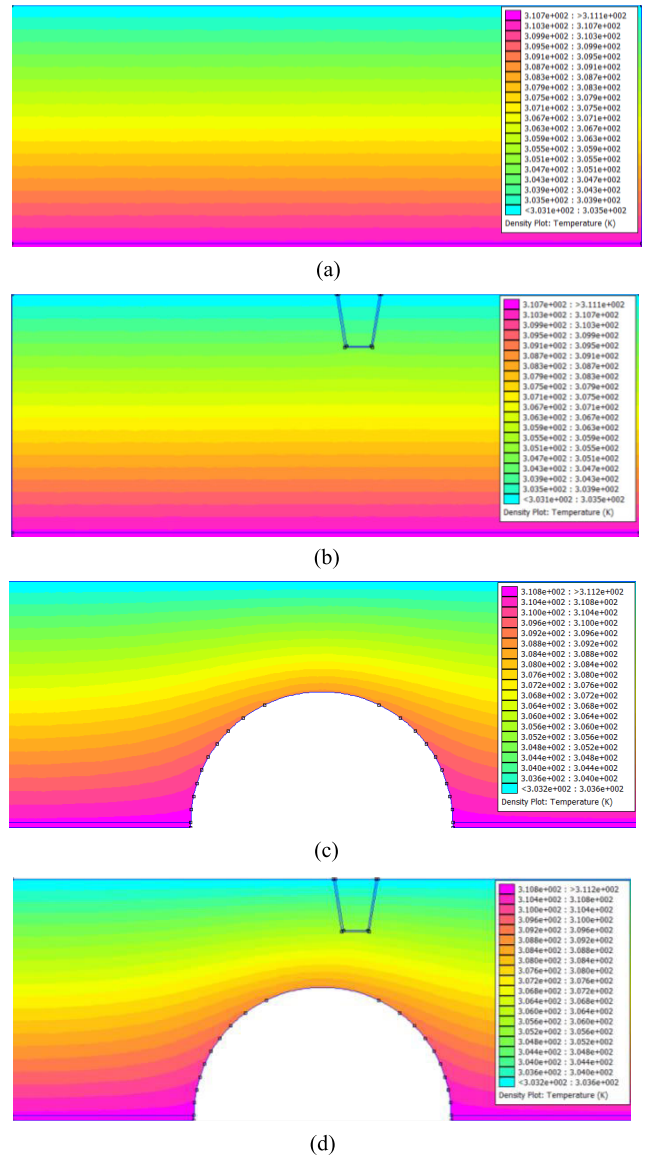


FIGURE 8. Heat flow diagrams in four conditions: (a) without a leakage (b) without a leakage and insulation installed (c) with a leakage (d) with a leakage and insulation installed.

the effect of the leak and that of the cup independently. Thus, there will be four heat flow diagrams as shown in Fig. 8.

VI. RESULTS

A. SIMULATION RESULTS

Using the Plot tool in FEMM, the temperature along the surface at a depth of 2 cm, which is the depth of the sensor in the hard prototype, in the four heat flow diagrams was graphed as shown in the Fig. 9. Since the model is symmetric, the temperature was read from the center till the right end of the model. In no leakage condition, the addition of the insulator introduced a disruption in the temperature along the surface where the difference between the temperature in the middle of the model and in the middle of the insulator,

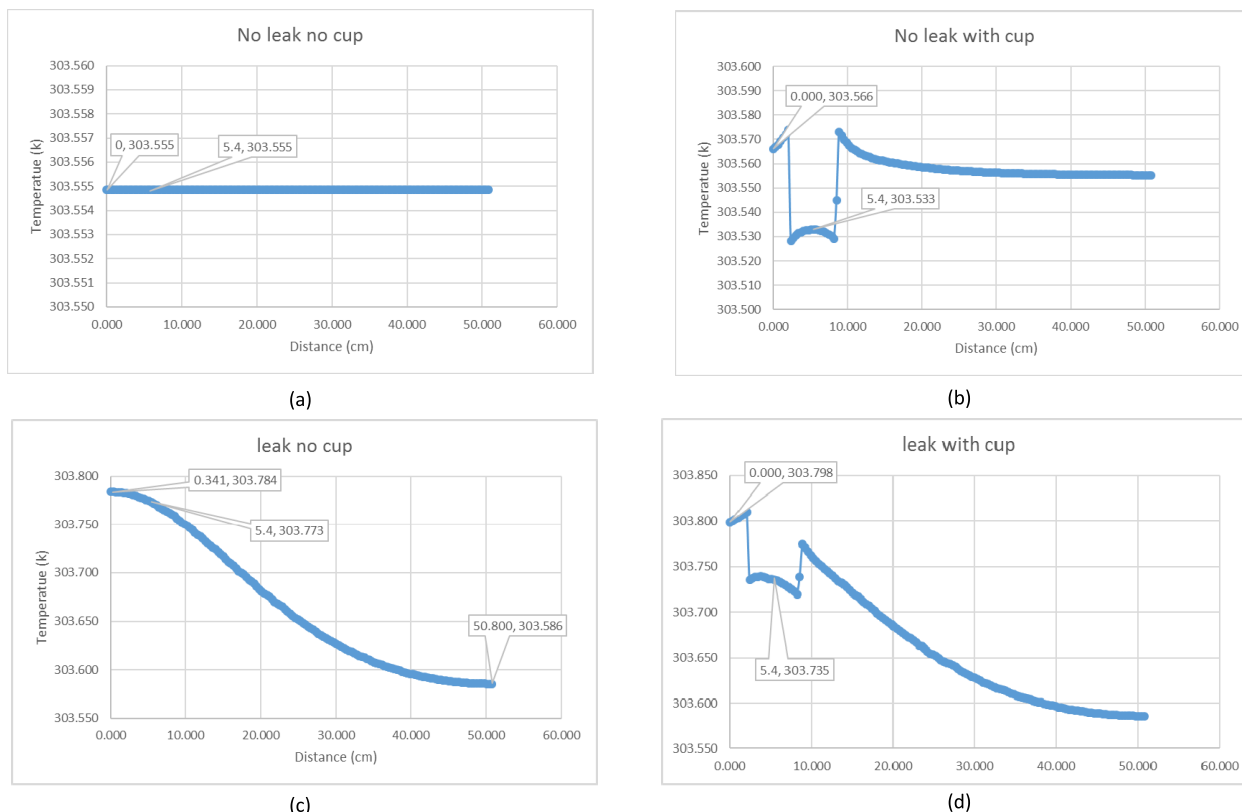


FIGURE 9. The temperature along the surface at a depth of 2 cm from the center until the far-right end for the four conditions shown in Fig. 4 in the same order.

which are the locations of the sensors in the hard prototype, is 0.033 K (°C), as shown in Fig. 9 (a,b). The leakage model shows that the addition of the cup increased that difference from 0.011 to 0.063 K (°C) when there is a leakage, as shown in Fig. 9 (c,d), thus, the disruption became more noticeable. Graphs also show that the further the sensor is from the center of the leakage location, the less temperature it will be detecting and, thus, the disruption in temperature along the surface will be more detectable. In normal condition, when there is no insulator, the difference between the maximum and minimum points is 0.198 K (°C), as Fig. 9 (c) shows. Although the widely used AAT sensor, LM35, cannot detect a small temperature difference of 0.198 K (°C) accurately where its readings' accuracy is within ± 0.5 °C, it still has a potential as its resolution is 0.01 °C and it has been used previously for leakage detection purposes [14]. Therefore, LM35 sensors are used in the experimental part of this project as explained in the next subsection.

B. EXPERIMENTAL RESULTS

The testing of the temperature sensing system was carried in two consecutive sunny days of similar weather conditions during sun peak hours, between 2 pm and 3:30 pm, so that maximum amount of leaked water evaporates maximizing the change in the temperature of the surrounding sand. In the first day, the temperature difference between the readings of the two sensors was measured without operating the pump

and it was noticed to vary between 0 and 0.5 °C, which equals the expected error in temperature reading according to the accuracy of the LM 35 sensor [23]. In the second day, the pump connected to the damaged pipeline in the prototype was operated, and the maximum temperature difference read was 1.47 °C after 30 minutes of operating the pump before this difference started to decrease to zero after one hour. To be more precise, when the difference between the readings of the two LM 35 sensors was maximum (1.47 °C), temperature of the thermally insulated sand was 30.76 °C, while in the adjacent open area, it was 32.23 °C. The temperature of the open area was expected to be higher than the insulated part as water temperature during the experiment was around 38 °C, which is in the range of the real water temperature in the WDN in Sharjah as shown in Fig. 10. Since the leaked water temperature in the prototype was higher than that of sand, it seems to have increased sand's surface temperature. The rebalancing in the system happened probably because of heat leaking to the insulated part through the polystyrene foam barrier, which does not represent a perfect thermal insulation or due to the decrease in the ambient temperature.

VII. DISCUSSION

A. SENSING NODE COVERAGE AREA

Because in actual condition the distance of leak from the sensors is unknown, the insulated sensor is preferred to be placed adjacent to the pipeline instead of being exactly above

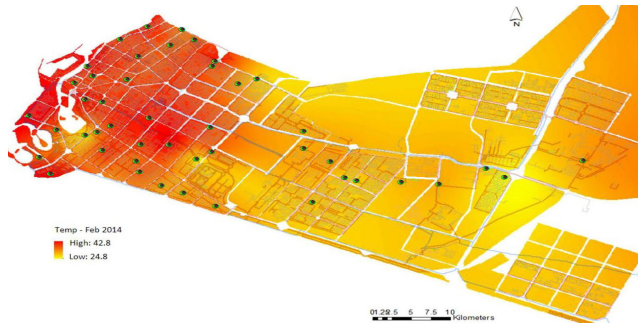


FIGURE 10. Distribution of water temperature within the WDN for Feb 2014 [44].

it to avoid data reading repetition between the two sensors, resulting in potentially erroneous zero leakage detection and to maximize the difference between the two readings. The coverage area of each sensor node depends on the radius of the resultant temperature anomaly on the surface above the leaking point. In worst case scenario, which was tested in the conducted experiments discussed previously, the leak is directly below the sensors. Thus, the area of the temperature anomaly will be covering both sensors. In this case, the sensor node proved to be effective. However, in the graphs in Fig. 7 and Fig. 11, it is shown that the thermal effect of leaked water diminishes rapidly as the distance increases from the leaking point. For example, the radius of the temperature anomaly depicted in Fig. 11, deduced from plot B, is around 5 cm, where the blue curve in the profile, which represents the temperature along the line crossing the anomaly, shows that between the center of the anomaly, at location 301 mm, and location 351 mm, the temperature will be always almost below 30 °C, which is 1.5 °C less than the temperature at the adjacent surface which fluctuates around 31.5 °C on both sides. Therefore, this suggests that if the horizontal distance between the leakage and sensing node, specifically the uninsulated sensor above the pipeline, is more than 5 cm, the leakage might not be detected, taking in consideration the similarity between the WDN prototype used in this paper and the one in Fig. 11. Moreover, in real life the amount of leaked water from WDN is much larger than the one presented in prototypes, where a pipe burst can even appear on the surface. Then, as a projection, if we multiply

the scale factor deduced in the Research Methodology section (4.92), with the approximated maximum distance of detection (5 cm), the maximum horizontal distance of detection turns to be 24.6 cm. In terms of depth, in the used prototype in this paper, the pipe was buried at a depth of almost 40.6 cm, which is similar to the distance between the temperature sensor and monitored pipe in [14] (30 cm). After scaling, in real life the system is expected to work at a depth of 2 m. Surely, if the pipeline is buried below 2 m, the depth upon which the scaling was set, the horizontal coverage area of the sensing node is expected to decrease where the heat flow diagrams in Fig. 8 shows that as it is further from the leakage the temperatures along horizontal layers tends to be closer. Although the rate of leaking water depends on the size of the breach in the pipe’s wall, this is not expected to affect the radius of the temperature anomaly very much where the amount of leaked water is also limited to the retention of the surrounding soil. To sum up, in order to further examine the system reliability, it should be used in more realistic setups. To improve the system’s sensitivity, they can be equipped with sensors with higher accuracy, such as LMT70 that has a maximum accuracy of $\pm 0.2^{\circ}\text{C}$ from -20°C to 90°C [54], to ensure a bigger margin between that the detected differences on the surface from system errors (fluctuation in the reading or self-heating of the buried sensors).

B. EFFECT OF ENVIRONMENTAL CONDITIONS

To further investigate the consistency of the system’s performance, it should be tested in different times along the year so that the effect of different temperature and humidity and other extreme conditions is explored. Among the most extreme environmental conditions in UAE is fog and sandstorms, where in addition to the mechanical power of the wind, they can diffract the laser beam through which the alarm signal is delivered. A sandstorm in UAE can last for several hours [55], while the fog often clears within about two hours after sunrise [56]. Finally, in the eastern part of UAE, where the city under study, Sharjah, is located, a heavy rainfall is expected to last for several minutes, while a light rainfall usually continues for a couple of hours [57]. Unusually, a heavy rainfall might last for more than two hours [58]. Thus, taking in consideration all the previous weather conditions, two solutions can be applied: the simple one is programing the sensing node to emit the alarm beam repetitively along the day and night, whereas the second is integrating fog and dust detection sensors to delay sending the alarm signal after the environmental event ends. Fog and rain can be detected by simple humidity sensors, but the high cost of dust sensors makes the second solution less preferable than the first one especially in the case of wide monitored area [59]. A through study of the effect of those environmental conditions on the propagation loss in case of using an RF communication system is recommended if it is considered as an alternative. Over the long term, to avoid the accumulation of sand on the laser diode, it can be fixed on a porous sheet instead of the solid one used [60]. The microprocessor can be buried in a plastic

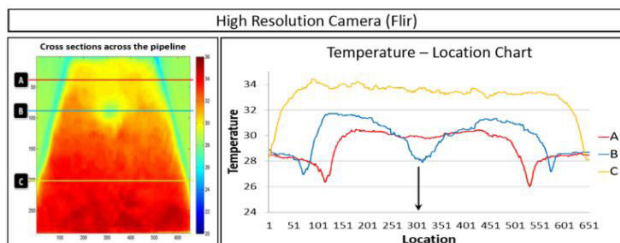


FIGURE 11. A high-resolution IR image and the associated temperature profiles [10].

case like the sensing node in [14], and to avoid the grounding of the temperature sensors which can defect its readings, due to a large leak or rainfall, waterproof LM35 sensors, which are commercially available, are suggested.

C. TECHNICAL COMPARISON

According to the profile in Fig. 11, the temperature difference between locations directly above the leaking section of a buried pipeline at a depth of 110 mm and horizontally adjacent points was around 4 °C in [10], which is comparable to the maximum temperature difference recorded in this paper (1.47 °C). In the experiments in [10], water had a temperature lower than that of the soil, and thus leaked water decreased the temperature at the surface, where the prototype was simulating the case of water being pumped from deep wells into the Great Man-made River of Libya which has lower temperature than that at the surface, unlike our case, where water mostly comes from desalination plants located above the surface. From the depiction of the experimental test rig in [10, Fig. 2], it can be deduced that the length of the buried pipeline was 525 mm. The IR camera could have been fixed high enough to cover wider area, but this needs experimental validation. Thus, according to the experimental results, two cameras would be needed per meter, whereas, according to the estimated coverage area of the proposed system, 25 sensing nodes would be needed per meter. Although both systems are costly when a large number of nodes are required to monitor a pipeline that extends for thousands of kilometers, the first one is more costly because of the high cost of the IR camera. Even though the need of large number of acoustic sensors and costly installation is an existing problem in acoustic leak detectors as well [61], [62], they are much more applicable than previously mentioned technologies where pressure pulses can be detected over a distance of several kilometers depending on the sensor used and location of deployment [63]. Another reason that makes acoustic detectors the most suitable solution in our case is its dependency on the physical vibration caused by the leak unlike the previous thermal detectors, which sense the surface's temperature that varies with weather fluctuations. However, the effectiveness of acoustic detectors can be limited by environmentally-induced uncertainties, such as external noise and demand variations [33]. Although the proposed model is only applicable for leak detection, the size of the leak can be estimated by counting the number of alarms in one area using the large number of sensing nodes. In this case, the location of each sensing node can be identified by the corresponding master node, which will be receiving the alarm, by assigning a specific time at which each node can send its alarm in accordance with a common network time protocol.

D. TOWARD DEVELOPING AUTONOMOUS SYSTEM

The proposed system would work more efficiently if it runs a comparison between the results of the FEMM simulation and sensors' readings automatically, where the deviation of

the sensors' readings from the resultant surface temperatures from the simulation with no leak condition can be used as a secondary indication of the existence of a leaks. To automatize the comparison of simulated and measured temperatures, the simulation must be written in Lua extension language, which is used to add scripting/batch processing facilities to FEMM [64], and the microprocessor must be replaced with a microcomputer, such as a Raspberry Pi 4, which can have an operating system, such as Windows, installed to run the FEMM program. There is no need for an additional sensor to measure the ambient temperature, which is one of the simulation parameters as discussed earlier in the subsection "PIPELINE SOFTWARE MODEL DEVELOPMENT," if it is to be taken from previous records of average temperatures like the ones in [65]. However, since the ambient temperatures changes annually [66], the error can increase in addition to the existing error because of the difference between the simulated (expected) and measured temperatures of soil in the open area where the proposed system was deployed above the pipeline, which was 1.582 °C, which corresponds to an percentage error of 0.049 %, when there was a leak.

VIII. CONCLUSION

In this paper, remote thermal water leakage sensing system with a laser communication system was introduced. A new system is proposed system consisting of a couple of AAT sensors, one installed at the surface, and the other was thermally insulated with the sand adjacent to it. The system was evaluated by computer simulation and experimental validation. The system was able to robustly detect leakage from a prototype WDN with a temperature uncertainty of ± 0.5 °C. The experimental testing of the proposed system showed ability to detect underground leakage.

APPENDIX

The program in the microcontroller of the proposed system in Arduino programming language:

```
int val;
int tempPin = 1;

void setup()
{
  pinMode(LED_BUILTIN, OUTPUT);
  Serial.begin(9600);
  pinMode(LED_BUILTIN, OUTPUT);
};

void loop()
{
  tempPin = 1;
  val = analogRead(tempPin);
  float mv = ( val/1024.0)*5000;
  float cell = mv/10;
  Serial.print("TEMPRATURE in insulated area = ");
```

```

Serial.print(ce11);
Serial.print("“*C”");
Serial.println();

++tempPin;
val = analogRead(tempPin);
mv = ( val/1024.0)*5000;
float cel2 = mv/10;
Serial.print("“TEMPRATURE in open area = ”");
Serial.print(ce12);
Serial.print("“*C”");
Serial.println();

if ((cel2 - cel1) >= 1.47) {
digitalWrite(LED_BUILTIN, HIGH);
delay(1);
digitalWrite(LED_BUILTIN, LOW);
delay(1);

delay(1800000);

}
}

```

REFERENCES

- [1] S. S. M. Ghafli and C. Morgan, "Challenges to the governance of water security in the UAE," M.S. thesis, Dept. Political Sci., United Arab Emirates Univ., Al Ain, United Arab Emirates, 2016.
- [2] *Leak Detection Services—Innovative Techniques, Money Back Guaranteed*. Accessed: Nov. 9, 2019. [Online]. Available: <https://digitalthermal.com/services/leak-detection-dubai/>
- [3] S. Renzetti and D. Dupont, "Buried treasure: The economics of leak detection and water loss prevention in Ontario," Environ. Sustainability Res. Centre, Brock Univ., Tech. Rep. ESRC-001-2013, Nov. 2019. [Online]. Available: <https://dr.library.brocku.ca/bitstream/handle/10464/4279/WorkingPaper-ESRC-2013-001.pdf?sequence=1&isAllowed=y>
- [4] U.S. Environmental Protection Agency, *Water Audits and Water Loss Control For Public Water Systems*. Accessed: Nov. 9, 2019. [Online]. Available: <https://www.epa.gov/sites/production/files/2015-04/documents/epa816f13002.pdf>
- [5] D. Ayala-Cabrera, E. Campbell, E. P. Carreño-Alvarado, J. Izquierdo, and R. Pérez-García, "Water leakage evolution based on GPR interpretations," *Procedia Eng.*, vol. 89, pp. 304–310, 2014. [Online]. Available: <https://doi.org/10.1016/j.proeng.2014.11.192>
- [6] Z. Liu and Y. Kleiner, "State of the art review of inspection technologies for condition assessment of water pipes," *Measurement*, vol. 46, no. 1, pp. 1–15, Jan. 2013.
- [7] S. Yazdekhasti, K. R. Piratla, J. C. Matthews, A. Khan, and S. Atamturktur, "Optimal selection of acoustic leak detection techniques for water pipelines using multi-criteria decision analysis," *Manage. Environ. Qual., Int. J.*, vol. 29, no. 2, pp. 255–277, Mar. 2018.
- [8] *Scottish Water Adopts New Phocus3 Acoustic Noise Logging For Effective Leak Location*. Accessed: May 30, 2020. [Online]. Available: <https://www.primayer.com/wp-content/uploads/2018/04/Phocus3-Scottish-Water-Case-Study-CS1-PH3-044-2.0.pdf>
- [9] C. Penteado, Y. Olivatti, G. Lopes, P. Rodrigues, R. Filev, and P. T. Aquino, "Water leaks detection based on thermal images," in *Proc. IEEE Int. Smart Cities Conf. (ISC2)*, Kansas City, MO, USA, Sep. 2018, pp. 498–505.
- [10] B. Shakmak and A. Al-Habaibeh, "Detection of water leakage in buried pipes using infrared technology; a comparative study of using high and low resolution infrared cameras for evaluating distant remote detection," in *Proc. IEEE Jordan Conf. Appl. Electr. Eng. Comput. Technol. (AEECT)*, The Dead Sea, Jordan, Nov. 2015, pp. 202–296.
- [11] M. Fahmy and O. Moselhi, "Detecting and locating leaks in underground water mains using thermography," in *Proc. Int. Symp. Autom. Robot. Construct. (ISARC)*, Austin, TX, USA, Jun. 2009, pp. 61–67.
- [12] C. Wang, M. Olson, B. Sherman, N. Dorjkhand, J. Mehr, and S. Singh, "Reliable leak detection in pipelines using integrated DdTS temperature and DAS acoustic fiber-optic sensor," in *Proc. Int. Carnahan Conf. Secur. Technol. (ICCST)*, Montreal, QC, Canada, Oct. 2018, pp. 1–5.
- [13] (2016). *Leak Detection Guarantees Pipeline Safety as Your Business Grows*. Accessed: Sep. 25, 2019. [Online]. Available: <https://www.yokogawa.com/library/resources/application-notes/pipeline-leak-detection/>
- [14] A. Sadeghioon, N. Metje, D. Chapman, and C. Anthony, "SmartPipes: Smart wireless sensor networks for leak detection in water pipelines," *J. Sensor Actuator Netw.*, vol. 3, no. 1, pp. 64–78, Feb. 2014.
- [15] Y. Li, C. Zhang, C. Chen, and H. Chen, "Calculation of capillary rise height of soils by SWCC model," *Adv. Civil Eng.*, vol. 2018, pp. 1–10, Aug. 2018.
- [16] *Thermacam P60: The Professional Thermographer's Choice*. Accessed: Nov. 14, 2019. [Online]. Available: <https://www.inspectahire.com/media/brochures/1400090001.pdf>
- [17] B. Liu, H. Ma, X. Zheng, L. Peng, and A. Xiao, "Monitoring and detection of combustible gas leakage by using infrared imaging," presented at the IEEE Int. Conf. Imag. Syst. Techn., Krakow, Poland, 2018.
- [18] A. Mishra and A. Soni, "Leakage detection using fibre optics distributed temperature sensing," presented at the 6th Int. Conf. Pipeline Technol. Conf., Hannover, Germany, vol. 5, 2011.
- [19] L. Wang, S. C. Narasimman, S. R. Ravula, and A. Ukil, "Water ingress detection in low-pressure gas pipelines using distributed temperature sensing system," *IEEE Sensors J.*, vol. 17, no. 10, pp. 3165–3173, May 2017.
- [20] A. Cataldo, G. Cannazza, E. De Benedetto, and N. Giaquinto, "A new method for detecting leaks in underground water pipelines," *IEEE Sensors J.*, vol. 12, no. 6, pp. 1660–1667, Jun. 2012.
- [21] A. Awwad, M. Yahyia, L. Albasha, M. M. Mortula, and T. Ali, "Communication network for ultrasonic acoustic water leakage detectors," *IEEE Access*, vol. 8, pp. 29954–29964, 2020.
- [22] *Remote Water Leakage Detection Utilising GPRS and 3G Communications*. Accessed: Aug. 3, 2019. [Online]. Available: <https://www.primayer.com/wp-content/uploads/2018/04/Phocus3-Scottish-Water-Case-Study-CS1-PH3-044-2.0.pdf>
- [23] *LM35 Precision Centigrade Temperature Sensors, SNIS159H Datasheet*, Texas Instruments, Aug. 1999, Revised: Dec. 2017.
- [24] J.-H. Park, "Anomaly detection from the signal of low-cost laser device without the false alarm and the missing," *IEEE Sensors J.*, vol. 18, no. 10, pp. 4275–4285, May 2018.
- [25] L. Pancheri and D. Stoppa, "A low-cost picosecond laser module for time-resolved optical sensing applications," *IEEE Sensors J.*, vol. 11, no. 6, pp. 1380–1381, Jun. 2011.
- [26] J. Boucart, "Laser diodes for (3D) sensing," in *Proc. Swiss Photon. Meeting, Industrial 3D Vision. Topic*, Jun. 2008, pp. 1–18.
- [27] M. Ali, L. Albasha, and H. Al-Nashash, "A Bluetooth low energy implantable glucose monitoring system," in *Proc. 41st EuMC*, Manchester, U.K., 2011, pp. 1265–1268.
- [28] N. A. Quadir, M. Taghadosi, L. Albasha, and N. Qaddoumi, "Design of self powered chip integrated humidity sensor," in *Proc. IEEE 59th Int. Midwest Symp. Circuits Syst. (MWSCAS)*, Abu Dhabi, UAE, Oct. 2016, pp. 1–4.
- [29] N. A. Quadir, L. Albasha, M. Taghadosi, N. Qaddoumi, and B. Hatahet, "Low-power implanted sensor for orthodontic bond failure diagnosis and detection," *IEEE Sensors J.*, vol. 18, no. 7, pp. 3003–3009, Apr. 2018.
- [30] X. Tan, Z. Sun, and I. F. Akyildiz, "A testbed of magnetic induction-based communication system for underground application," *IEEE Antennas Propag. Mag.*, to be published.
- [31] K. A. U. Menon, A. Gungi, and B. Hariharan, "Efficient wireless power transfer using underground relay coils," in *Proc. 5th Int. Conf. Comput., Commun. Netw. Technol. (ICCCNT)*, Hefei, China, Jul. 2014, pp. 1–5.
- [32] B. Griffin and C. Detweiler, "Resonant wireless power transfer to ground sensors from a UAV," in *Proc. IEEE Int. Conf. Robot. Autom.*, Saint Paul, MN, USA, May 2012, pp. 2660–2665.
- [33] S. N. U. Saqib, M. F. Mysorewala, and L. Cheded, "A multiscale approach to leak detection and localization in water pipeline network," *Water Resour. Manage.*, vol. 31, no. 12, pp. 3829–3842, May 2017.
- [34] X. J. Wang, R. Y. Li, and J. S. Chen, "Concentrated-leakage detection by emulation of temperature field," *Appl. Mech. Mater.*, vol. 224, pp. 93–96, Nov. 2012.

- [35] M. Golmohamadi, "Pipeline leak detection," M.S. thesis, Dept. Comp. Eng. Mech. Eng., Missouri Univ., Columbia, MO, USA, 2015.
- [36] O. Begovich and A. Pizano-Moreno, "Application of a leak detection algorithm in a water pipeline prototype: Difficulties and solutions," in *Proc. 5th Int. Conf. Electr. Eng., Comput. Sci. Autom. Control*, Mexico City, Mexico, Nov. 2008, pp. 26–30.
- [37] T. S. T. Amran, M. P. Ismail, M. R. Ahmad, M. S. M. Amin, M. A. Ismail, S. Sani, N. A. Masenwat, and N. S. M. Basri, "Monitoring underground water leakage pattern by ground penetrating radar (GPR) using 800 MHz antenna frequency," in *Proc. iNuSTEC*, Johor Bahru, Malaysia, vol. 298, 2018, Art. no. 012002.
- [38] A. Martini, M. Troncosi, and A. Rivola, "Leak detection in water-filled small-diameter polyethylene pipes by means of acoustic emission measurements," *Appl. Sci.*, vol. 7, no. 1, p. 2, Dec. 2016.
- [39] M. J. Brennan, P. F. Joseph, J. M. Muggleton, and Y. Gao, "Some recent research results on the use of acoustic methods to detect water leaks in buried plastic water pipes," *Inst. Sound Vibration Res.*, Univ. Southampton, Southampton, U.K., 2008.
- [40] H. Aslam, M. Kaur, S. Sasi, M. Mortula, S. Yehia, and T. Ali, "Detection of leaks in water distribution system using non-destructive techniques," in *Proc. ICREE*, Phuket, Thailand, 2018, Art. no. 012004.
- [41] H. Aslam, M. Kaur, M. Mortula, and T. Ali, "A conceptual approach to detection of water pipe leakage using non destructive techniques," presented at the 5th Int. Conf. Water, Energy Environ., Sharjah, UAE, vol. 2, 2017.
- [42] J. N. Damask, *Polarization Optics in Telecommunications*. New York, NY, USA: Springer, 2011, p. 222.
- [43] M. Brinson and V. Kuznetsov, "Qucs-0.0.19S: A new open-source circuit simulator and its application for hardware design," in *Proc. Int. Siberian Conf. Control Commun. (SIBCON)*, Moscow, Russian, May 2016, pp. 1–5.
- [44] M. M. Mortula, T. A. Ali, R. Sadiq, A. Idris, and A. Al Mulla, "Impacts of water quality on the spatiotemporal susceptibility of water distribution systems," *CLEAN—Soil, Air, Water*, vol. 47, no. 5, May 2019, Art. no. 1800247.
- [45] *Arduino Uno Datasheet*, Farnell, London, U.K., 2012.
- [46] *Analogread*. Accessed: Nov. 13, 2019. [Online]. Available: <https://www.arduino.cc/reference/en/language/functions/analog-io/analogread/>
- [47] R. Alley. (Mar. 2018). *Energizer Watt-Hour Battery Specs*. Accessed: Nov. 14, 2019. [Online]. Available: <https://sciencing.com/energizer-watthour-battery-specs-7425932.html>
- [48] *Thermal Properties*. [Online]. Available: https://www.mep.co.jp/en/pdf/product/iupi_nova/physicality_04.pdf
- [49] *Expanded Polystyrene (EPS): Ultimate Guide on Foam Insulation Material*. Accessed: Mar. 12, 2020. [Online]. Available: <https://omnexus.specialchem.com/selection-guide/expanded-polystyrene-eps-foam-insulation>
- [50] R. Salim, "Extent of capillary rise in sands and silts," M.S. thesis, Geosci. Dept. Western Michigan Univ., Kalamazoo, MI, USA, 2016.
- [51] R. Kodešová, M. Vlasáková, M. Fér, D. Teplá, O. Jakšík, P. Neuberger, and R. Adamovský, "Thermal properties of representative soils of the Czech Republic," *Soil Water Res.*, vol. 8, no. 4, pp. 141–150, Oct. 2013.
- [52] L. Chiapponi, "Water retention curves of multicomponent mixtures of spherical particles," *Powder Technol.*, vol. 320, pp. 646–655, Oct. 2017.
- [53] M. Tuller and D. Or, "Retention of water in soil and the soil water characteristic curve," in *Encyclopedia of Soils in the Environment*. Amsterdam, The Netherlands: Elsevier, 2004, pp. 278–289. [Online]. Available: https://www.researchgate.net/publication/251875388_Water_retention_and_characteristic_curve
- [54] *LMT70, LMT70A ±0.05 °C Precision Analog Temperature Sensor, RTD and Precision NTC Thermistor IC, SNIS187A datasheet*, Texas Instrum., Dallas, TX, USA, Mar. 2015.
- [55] *National Center of Meteorology & Seismology, Dust Sources Affecting the United Arab Emirates*. Ministry Presidential Affairs, Abu Dhabi, United Arab Emirates, 2011.
- [56] M. P. de Villiers and J. van Heerden, "Fog at Abu Dhabi international airport," *Weather*, vol. 62, no. 8, pp. 209–214, 2007.
- [57] M. Sherif, R. Chowdhury, and A. Shetty, "Rainfall and intensity-duration-frequency (IDF) curves in the United Arab Emirates," in *Proc. World Environ. Water Resour. Congr.*, Portland, OR, USA, May 2014, pp. 2316–2325.
- [58] Khaleej Times.(Jan. 2020). *Revealed: Just How Much Rain Did Dubai Receive?* Accessed: May 21, 2020. [Online]. Available: <https://www.khaleejtimes.com/news/weather/revealed-just-how-much-rain-did-dubai-receive>
- [59] M. Akhlaq, T. R. Sheltami, and H. T. Mouftah, "A review of techniques and technologies for sand and dust storm detection," *Rev. Environ. Sci. Bio/Technol.*, vol. 11, no. 3, pp. 305–322, Sep. 2012.
- [60] L. Bruno, M. Horvat, and L. Raffaele, "Windblown sand along railway infrastructures: A review of challenges and mitigation measures," *J. Wind Eng. Ind. Aerodynamics*, vol. 177, pp. 340–365, Jun. 2018.
- [61] K. B. Adedeji, Y. Hamam, B. T. Abe, and A. M. Abu-Mahfouz, "Towards achieving a reliable leakage detection and localization algorithm for application in water piping networks: An overview," *IEEE Access*, vol. 5, pp. 20272–20285, 2017.
- [62] H. Ali and J.-H. Choi, "A review of underground pipeline leakage and sinkhole monitoring methods based on wireless sensor networking," *Sustainability*, vol. 11, no. 15, p. 4007, Jul. 2019.
- [63] I. Stoianov, L. Nachman, S. Madden, and T. Tokmouline, "PIPENET: A wireless sensor network for pipeline monitoring," in *Proc. 6th Int. Symp. Inf. Process. Sensor Netw.*, Cambridge, MA, USA, Apr. 2007, pp. 264–273.
- [64] D. Meeker, "Lua scripting," in *Finite Element Method Magnetics Version 4.2 User's Manual*, vol. 1. DL-Manual, 2015, ch. 3, sec. 1, p. 82. [Online]. Available: <http://www.femm.info/Archives/doc/manual.pdf>
- [65] Statistics Centre, Abu Dhabi, UAE. (2020). *Statistical Yearbook of Abu Dhabi 2020*. [Online]. Available: https://www.scad.gov.ae/Release%20Documents/Statistical%20Yearbook%20of%20Abu%20Dhabi_2020_Annual_Yearly_en.pdf
- [66] A. U. Komuscu, "Long-term mean monthly temperatures trends of the United Arab Emirates," *Int. J. Global Warming*, vol. 11, no. 1, pp. 1–22, 2017.



AMEEN AWWAD received the B.Sc. degree from the American University of Sharjah, in 2019. He is currently a Researcher with the Electrical Engineering Department, American University of Sharjah (AUS). His research areas are wireless power transfer, energy harvesting, and leakage detection.



MOHAMED YAHYA received the B.Sc. and M.Sc. degrees from the Higher School of Sciences and Techniques, Tunis, Tunisia, in 2000 and 2002, respectively, the Ph.D. degree in telecommunication engineering conjointly from the National Engineering School of Gabes (NESG), Tunisia, and the Ecole Nationale Supérieure d'Electrotechnique, d'Electronique, d'Informatique, d'Hydraulique et des Télécommunications (ENSEEIH), Toulouse, France, in 2010, and the

Habilitation degree in telecommunications from the University of Gabes, Tunisia, in 2017.

In 2018, he has been an Associate Professor with NESG. In 2019, he is a Postdoctoral Research Associate with the American University of Sharjah. His current research interests include analysis of polarimetric SAR images and numerical methods in electromagnetism.



LUTFI ALBASHA (Senior Member, IEEE) received the B.Eng. and Ph.D. degrees in electronic and electrical engineering from the University of Leeds, U.K. He joined Sony Corporation, in 1997, where he was involved in designing commercial RFIC chip products for mobile handsets. He joined Filtronic Semiconductors, in 2000, as a Senior Principal Engineer, and created and managed its IC design team. The team supported the company foundry design enablement for mass production of RFIC products and taped-out its first commercial chips. This becomes a very successful business in Europe's largest GaAs MMIC foundry. He returned to Sony as a Lead Principal Engineer, where he was involved in highly integrated RFCMOS and BiCMOS transceivers for cellular and TV applications. He joined the American University of Sharjah, where he progressed to rank of Professor of electrical engineering. His current areas of research are in energy harvesting and wireless power transfer, low-power wearable and implantable devices, power amplifier design and linearization, and miniaturized digital radar transceivers. He has received several outstanding recognition awards from Sony Corporation, the IET, IEEE, and the University of Leeds. He is an Associate Editor of the *IET Microwaves, Antenna and Propagation Journal* and served for three terms as the President of the UAE Chapter of the IEEE Solid-State Circuits Society.



TARIG ALI (Senior Member, IEEE) received the B.S. degree (Hons.) in civil engineering from the University of Khartoum, Sudan, in 1993, and the M.S. and Ph.D. degrees from Ohio State University, USA, in 1999 and 2003, respectively. He is currently an Associate Professor with the American University of Sharjah. His research areas include geospatial engineering, GIScience, coastal mapping and GIS, and applications of GIS and remote sensing in civil and environmental engineering.

...



MD. MARUF MORTULA received the B.Sc. degree from the Bangladesh University of Engineering and Technology, Bangladesh, in 2000, and the M.Sc. and Ph.D. degrees from Dalhousie University, Canada, in 2002 and 2006, respectively. Since 2018, he has been a Full Professor with the American University of Sharjah. His research areas are water and wastewater treatment, recycling of solid waste management, water quality management in coastal water, water infrastructure management, and water distribution systems.